

Electronic Supplementary Material (ESI) for Journal of Materials Chemistry A.
This journal is © The Royal Society of Chemistry 2021

Electronic Supplementary Material (ESI)

Zinc/Graphitic carbon nitride co-mediated dual-template synthesis of densely populated Fe-N_x embedded 2D carbon nanosheets towards oxygen reduction reaction for Zn-air batteries

Xiao-Fei Gong^a, Yun-Long Zhang^a, Lei Zhao*^a, Yun-Kun Dai^a, Jia-Jun Cai^a, Bing
Liu^a, Pan Guo^a, Qing-Yan Zhou^a, Ichizo Yagi^c, Zhen-Bo Wang*^{a, b}

^a MIIT Key Laboratory of Critical Materials Technology for New Energy Conversion
and Storage, State Key Lab of Urban Water Resource and Environment, School of
Chemistry and Chemical Engineering, Harbin Institute of Technology, Harbin,
150001 China.

^b College of Materials Science and Engineering, Shenzhen University, Shenzhen
518071, Guangdong, China.

^c Faculty of Environmental Earth Science, Graduate School of Environmental Science,
Hokkaido University, N10W5, Kita-ku, Sapporo 060-0810, Japan

*corresponding author. E-mail: leizhao@hit.edu.cn, wangzhb@hit.edu.cn

Experimental Section

Materials

Melamine, D-glucosamine hydrochloride, ferrous sulfate heptahydrate ($\text{FeSO}_4 \cdot 7\text{H}_2\text{O}$, $\geq 99.0\%$), Zinc chloride (ZnCl_2 , $\geq 98.0\%$) and potassium hydroxide (KOH, 95%) were purchased from Aladdin (Shanghai, China). Sulfuric acid (H_2SO_4) was purchased from Kermel. Nafion solution (5 wt%) was bought from Sigma-Aldrich. Carbon supported Pt (Pt/C, 20 wt% Pt) was bought from Johnson Matthey Corp. All the reagents were used without further purification.

Synthesis of Fe-SAs/N-CNSs and the contrastive samples.

Firstly, the C_3N_4 precursor was synthesized via pyrolyzing 2.00 g of melamine at 550 °C for 2 h under Ar. Subsequently, 300 mg of C_3N_4 , 500 mg of D-glucosamine hydrochloride, 50 mg of $\text{FeSO}_4 \cdot 7\text{H}_2\text{O}$ and 50 mg of ZnCl_2 were dispersed in 30 ml of deionized water and kept under sonication for 24 h to ensure homogenization. The above suspension was then dried at 60 °C overnight and the obtained light yellow powder was pyrolyzed at 900 °C for 2 h under Ar at a heating rate of 5 °C/min. Afterwards, the prepared black powder was acid leached in 0.5 M H_2SO_4 solution at 80 °C for 5 h followed by washed with deionized water several times, dried at 80 °C for 5 h and then pyrolyzed again at 900 °C for 2 h under Ar to obtain Fe-SAs/N-CNSs. For comparison, Fe-NPs/N-CNSs were prepared by the similar preparation process to that of the Fe-SAs/N-CNSs except for the acid washing process. In addition, N-CNSs were prepared under the same condition of Fe-SAs/N-CNSs but without the addition of $\text{FeSO}_4 \cdot 7\text{H}_2\text{O}$. And, bulk-Fe/N-C were synthesized through the similar preparation process to SAs-Fe/N-CNSs except the addition of $\text{g-C}_3\text{N}_4$. Meanwhile, a series of SAs-Fe/N-CNSs- x catalysts were synthesized by varying the molar ratio (x) of Zn salt to Fe salt ($x = 0, 1, 2, \text{ and } 4$) through the similar preparation process. Notably, the SAs-Fe/N-CNSs-2 sample is the sample denoted as SAs-Fe/N-CNSs in the above

discussion.

Physical Characterization

Transmission electron microscopy (TEM) employing FEI Tecnai G2 F20 was employed to investigate the morphology of the prepared samples. Then, high resolution transmission electron microscopy (HRTEM), high-angle annular dark-field scanning transmission electron microscopy (HAADF-STEM), and selected area electron diffraction (SAED) images were obtained with a JEM-2100F microscope (JEOL, Japan) at an operating voltage of 200 keV. Besides, the aberration corrected high-angle annular dark-field scanning transmission electron microscopy (AC HAADF-STEM) image was acquired with FEI Titan Cubed Themis G2 300 (Netherlands). Powder X-ray diffraction (XRD) measurements were performed by a D/max-RB diffractometer (made in Japan) using a Cu Ka X-ray source operating at 45 kV and 100 mA, scanning at a rate of $4^{\circ} \text{ min}^{-1}$. Nitrogen adsorption-desorption isotherms were obtained by Micromeritics ASAP 2020 instrument. The Raman spectra was recorded on a Renishaw1000 Raman microscope (Rhenishaw Instruments, England) using a 532 nm argon ion laser. Then, X-ray photoelectron spectroscopy (XPS) measurements were carried out on a physical electronics PHI model 5700 instrument, wherein the Al X-ray source was operated at 250 W and the take-off angle of the sample to analyzer was 45° . Additionally, all of the XPS results are calibrated by the peak position of C 1s spectra (284.6 eV).

Electrochemical Measurements

All of the electrochemical tests were carried out on a CHI 650E electrochemical workstation within a standard three-electrode system at room temperature. The counter electrode and reference electrode were Pt wire and Ag/AgCl (saturated KCl) electrode, respectively. Then, the working electrode was prepared as the following procedure: At first, 2.5mg of catalyst was dispersed into the mixed solution (500 μ L) of water/ethanol/0.1 wt% Nafion (volume ratio = 5:5:0.3) and then the resulting

homogeneous ink was obtained after ultrasonication for 1 h. Subsequently, 20 μ L of the catalyst ink was dropped onto a rotating ring-disk electrode (RRDE) with a glassy carbon (GC) disk of 5.6 mm in diameter. Finally, the target the working electrode was prepared after being dried at room temperature with a catalyst loading of 0.4 mg cm⁻¹. Note that all the measured potentials versus Ag/AgCl were converted to the potentials versus reversible hydrogen electrode (RHE).

Firstly, cyclic voltammetry (CV) curves were measured in Ar- or O₂-saturated 0.1 M KOH electrolyte within potentials of 0.00 V to 1.20 V at a scan rate of 50 mV s⁻¹. Note that the working electrode was cycled at 100 mV s⁻¹ in advance for the stability of the CV polarization curves. Rotating disk electrode (RDE) tests were employed to record the staircase voltammetry (SCV) curves with a potential step of 50 mV and step period of 30 s from 1.20 V to 0.00 V in O₂-saturated 0.1 M KOH or 0.5 M H₂SO₄ electrolyte at 1600 rpm. The stability of the catalysts was evaluated via current-time (i-t) chronoamperometric tests at 0.80 V in O₂-saturated 0.1 M KOH solution at 1600 rpm for 10000 s. The stability of the catalysts was also tested through the CV measurements in O₂-saturated 0.1 M KOH within the potential from 0.6 V to 1.0 V at 50 mV s⁻¹ for 5000 cycles. The methanol resistance experiments were performed by chronoamperometric measurement at 0.6 V by adding 3 M methanol into the electrolyte at about 400 s. Additionally, rotating ring-disk electrode (RRDE) techniques were also adopted to examine the electron transfer number (n) and H₂O₂ yield, which were calculated from the following equation:

$$H_2O_2(\%) = 200 \times \frac{\frac{I_R}{N}}{I_D + \frac{I_R}{N}}$$

$$n = 4 \times \frac{I_D}{I_D + \frac{I_R}{N}}$$

Here, I_D and I_R are the disk and ring currents, respectively, and N (~ 0.37) is the current collection efficiency of the Pt ring.

Electrochemical impedance spectroscopy (EIS) was performed in 0.1 M KOH by

applying an AC voltage with 5 mV amplitude in frequencies ranging from 1 Hz to 50 kHz. The specific data can be fitted by Zview software.

The Practical application potential of Fe/N-CNRs was manifested by primary Zn-air batteries with 6.0 M KOH aqueous solution as the electrolyte and polished Zn plate as the anode. The air cathode was consisted of the catalyst layer (CL) on the solution side and commercial gas diffusion layer (GDL) on the air side. Thereinto, the catalyst layer (CL) was prepared as follows: Fe/N-CNRs catalyst (2.5 mg), activated carbon (4 mg), acetylene black (1 mg), and Nafion (5 wt%, 8 μ l) were dispersed in 200 μ l of isopropyl alcohol to form a homogeneous catalyst ink by sonication for 45 min. Afterwards, the above catalyst ink was dropped onto the cleaned Ni foam (1.0 cm²) and then dried at 60 h for 12 h with catalyst loading of 2.5 mg cm⁻². For comparison, commercial 20% Pt/C catalyst was employed as air cathode catalyst following the same process. The polarization curve tests and galvanostatic discharge curves were acquired through the LAND CT2001A testing system. Besides, the specific capacity of Zn-air battery was derived from the following equation:

$$C_{sp} = \frac{i \times t}{\Delta m}$$

wherein i stands for the discharge current, t stands for the discharge time and Δm stands for the weight of the consumed zinc.

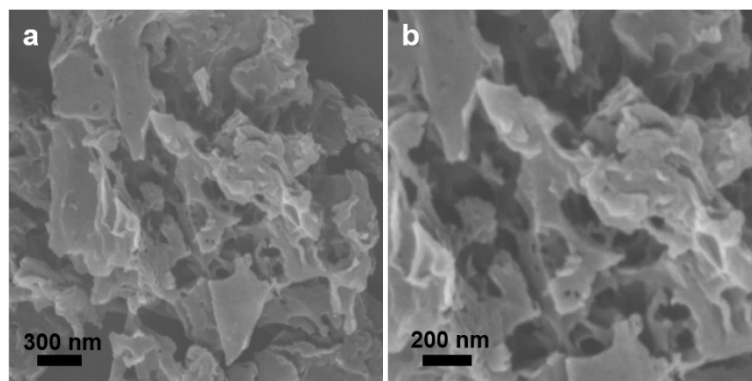


Fig. S1. a) SEM image and b) Enlarge SEM image of SAs-Fe/N-CNSs.

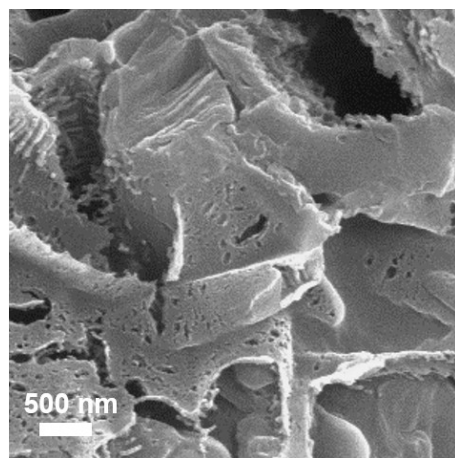


Fig. S2. SEM image of g-C₃N₄.

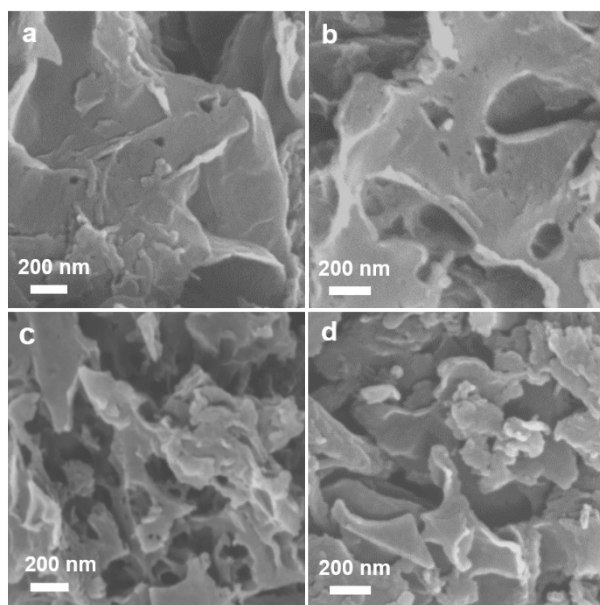


Fig. S3. SEM image of a) SAs-Fe/N-CNSs-0, b) SAs-Fe/N-CNSs-1, c) SAs-Fe/N-CNSs-2, and d) SAs-Fe/N-CNSs-4.

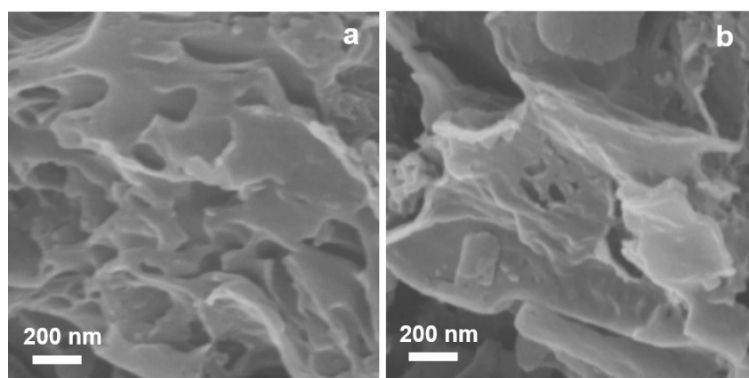


Fig. S4. SEM image of a) N-CNSs and b) NPs-Fe/N-CNSs.

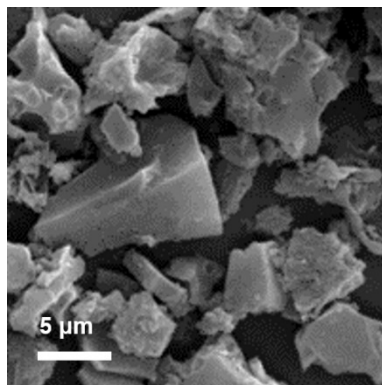


Fig. S5. SEM image of bulk-Fe/N-C without g-C₃N₄ template.

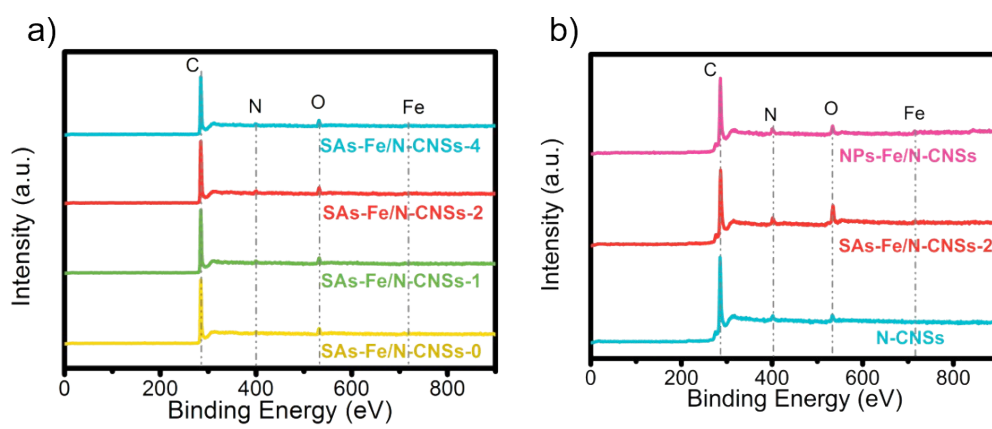


Fig. S6. a) XPS surveys of SAs-Fe/N-CNSs-0, SAs-Fe/N-CNSs-1, SAs-Fe/N-CNSs-2, and SAs-Fe/N-CNSs-4. b) XPS surveys of NPs-Fe/N-CNSs, SAs-Fe/N-CNSs-2, and N-CNSs.

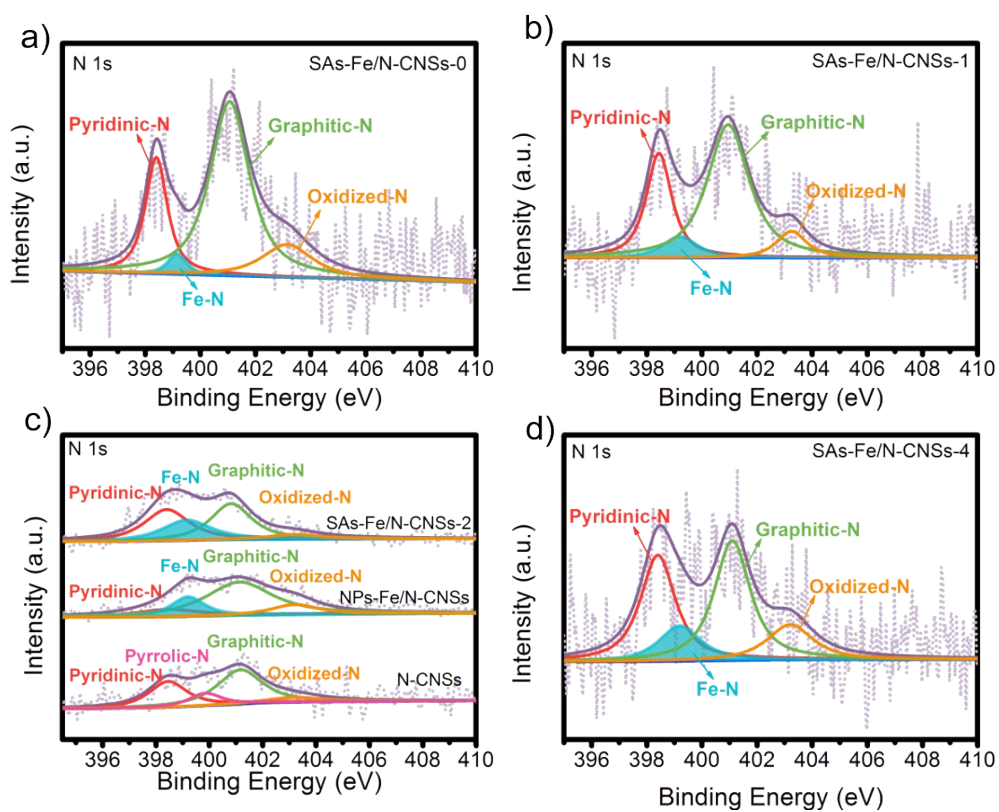


Fig. S7. XPS N 1s spectra of a) SAS-Fe/N-CNSs-0 and b) SAS-Fe/N-CNSs-1, c) XPS N 1s spectra of SAS-Fe/N-CNSs-2, NPs-Fe/N-CNSs, and N-CNSs, d) XPS N 1s spectra of SAS-Fe/N-CNSs-4.

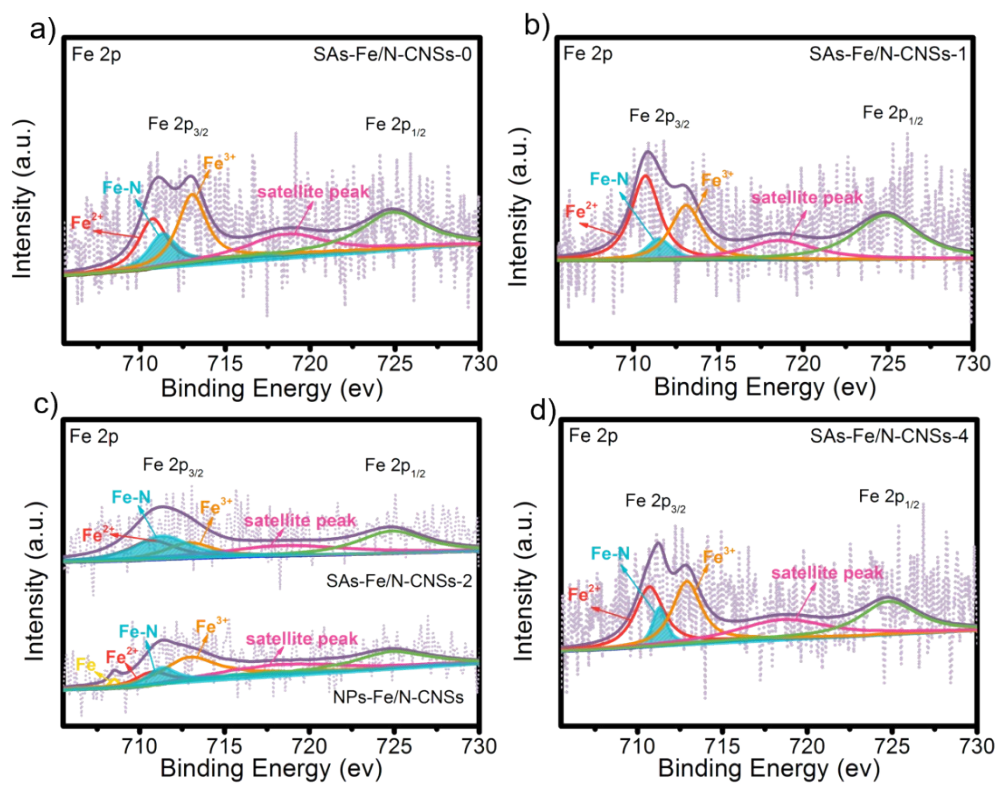


Fig. S8. XPS Fe 2p spectra of a) SAs-Fe/N-CNSs-0 and b) SAs-Fe/N-CNSs-1, c) XPS Fe 2p spectra of SAs-Fe/N-CNSs-2 and NPs-Fe/N-CNSs, d) XPS Fe 2p spectra of SAs-Fe/N-CNSs-4.

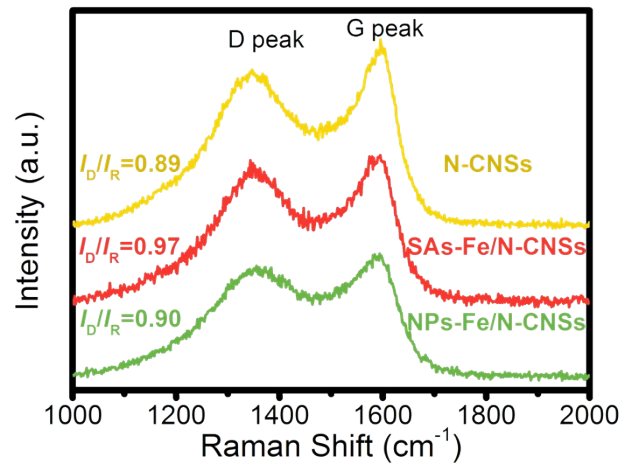


Fig. S9. Raman spectra of N-CNSs, SAs-Fe N-CNSs, and NPs-Fe N-CNSs.

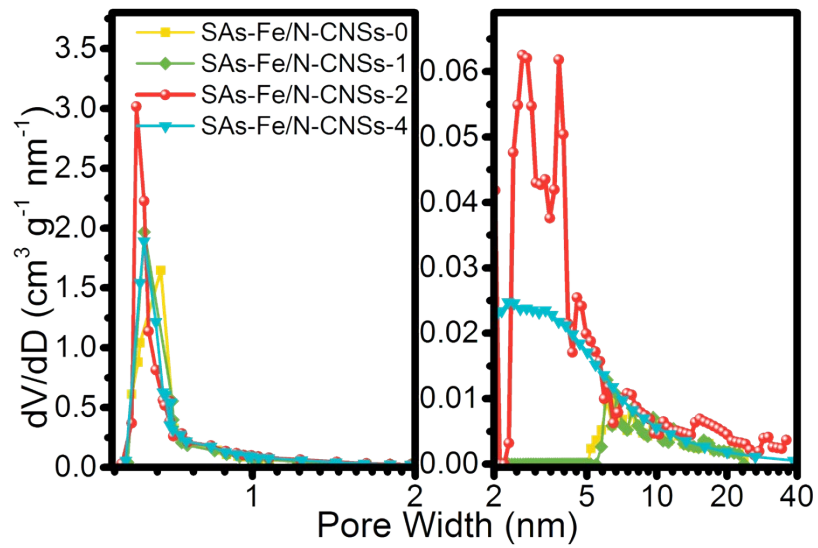


Fig. S10. Pore size distribution of SAs-Fe/N-CNSs-0, SAs-Fe/N-CNSs-1, SAs-Fe/N-CNSs-2 and SAs-Fe/N-CNSs-4.

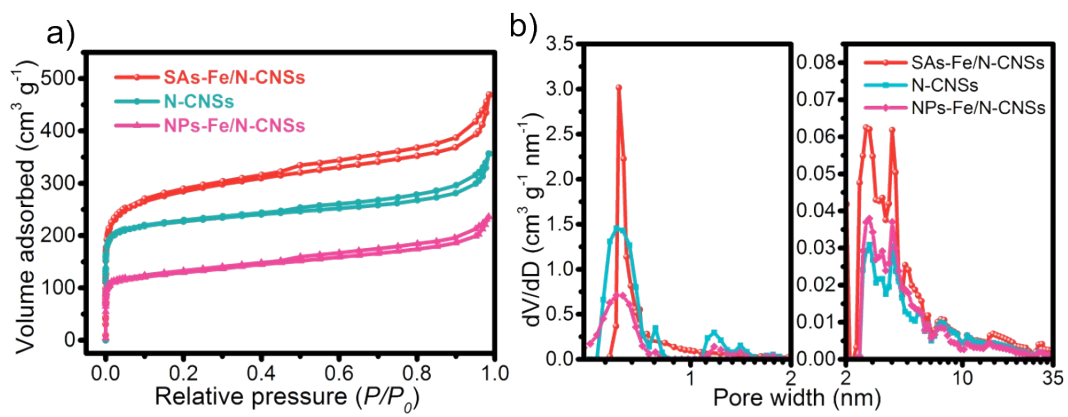


Fig. S11. (a) Nitrogen adsorption-desorption isotherms of SAs-Fe/N-CNSs, N-CNSs, and NPs-Fe/N-CNSs. (b) Pore size distribution of SAs-Fe/N-CNSs, N-CNSs, and NPs-Fe/N-CNSs.

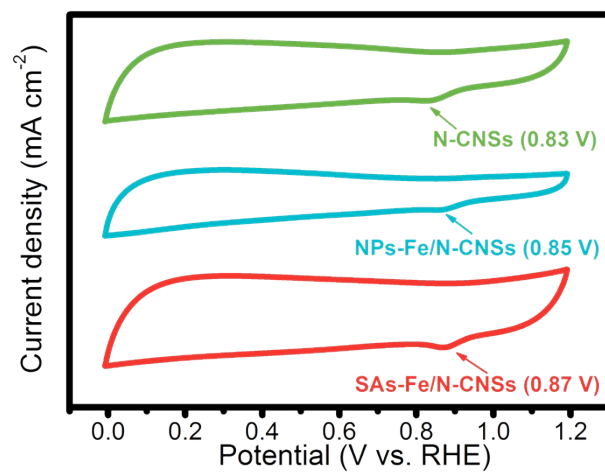


Fig. S12. CV curves of SAs-Fe/N-CNSs, NPs-Fe/N-CNSs and N-CNSs in O₂-saturated 0.1 M KOH solution.

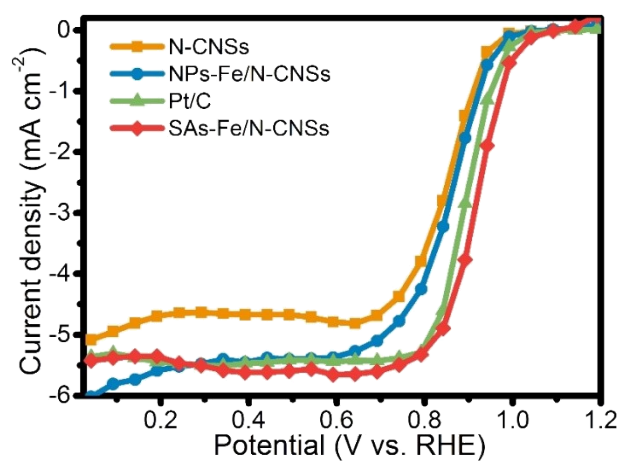


Fig. S13. SCV curves of N-CNSs, NPs-Fe/N-CNSs, Pt/C, and SAs-Fe/N-CNSs in O₂-saturated 0.1 M KOH solution.

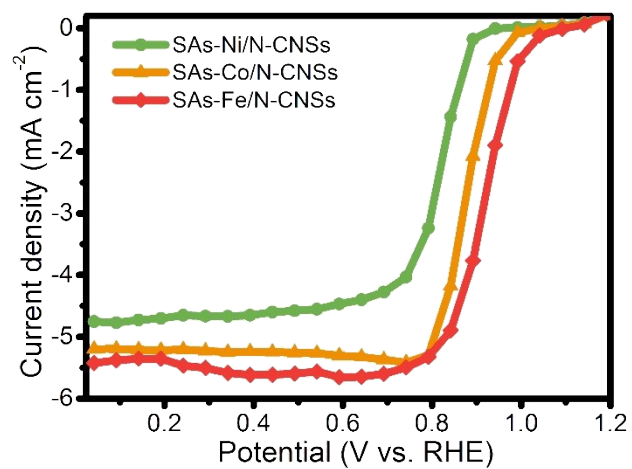


Fig. S14. SCV curves of SAs-Ni/N-CNSs, SAs-Co/N-CNSs, and SAs-Fe/N-CNSs in O₂-saturated 0.1 M KOH solution.

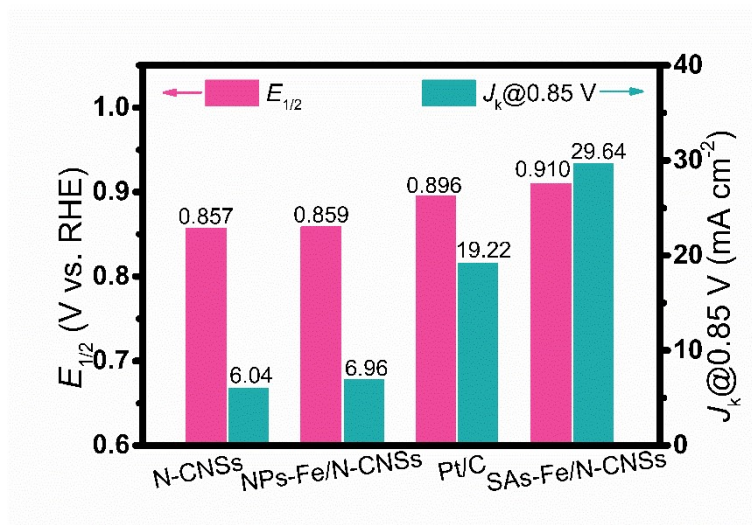


Fig. S15. $E_{1/2}$ and $J_k@0.85\text{ V}$ (J_k at 0.85 V) results of N-CNSs, NPs-Fe/N-CNSs, Pt/C, and SAs-Fe/N-CNSs in O_2 -saturated 0.1 M KOH solution.

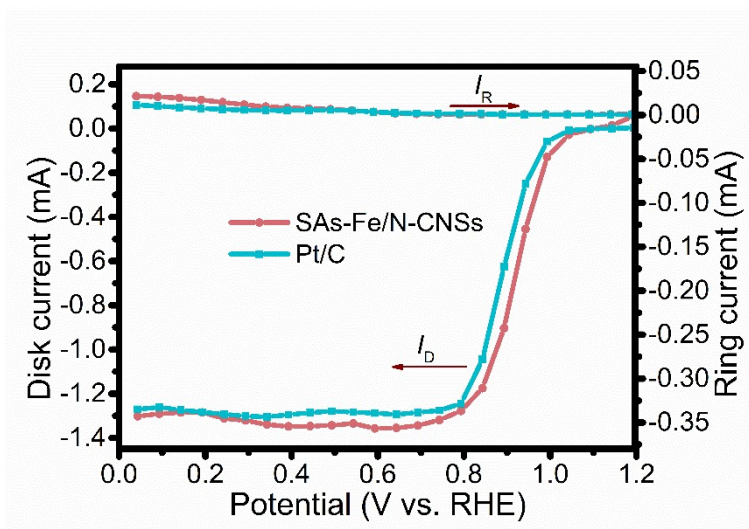


Fig. S16. The LSV plots of SAs-Fe/N-CNSs and Pt/C in disk and ring. (I_D : ring current, I_R : disk current).

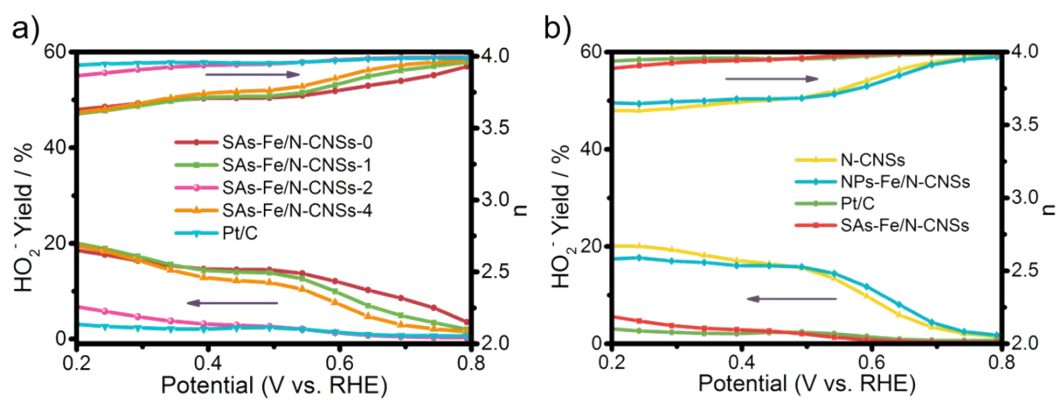


Fig. S17. Hydrogen peroxide yield and electron-transfer numbers of various catalysts in O_2 -saturated 0.1 M KOH solution.

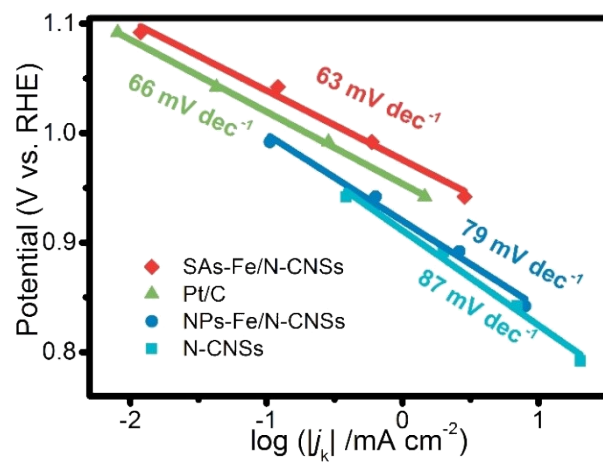


Fig. S18. Tafel slope of N-CNSs, NPs-Fe/N-CNSs, Pt/C, and SAs-Fe/N-CNSs in O₂-saturated 0.1 M KOH solution.

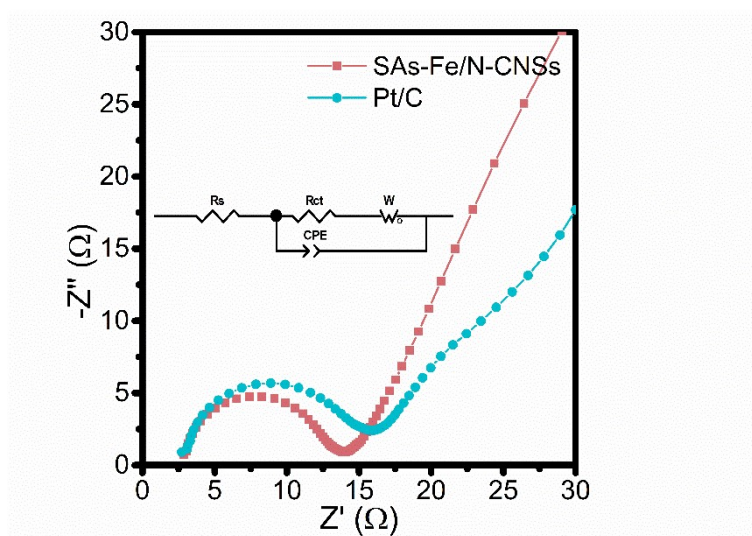


Fig. S19. Nyquist plots of electrochemical impedance spectroscopy (EIS) for SAs-Fe/N-CNSs and Pt/C in 0.1 M KOH.

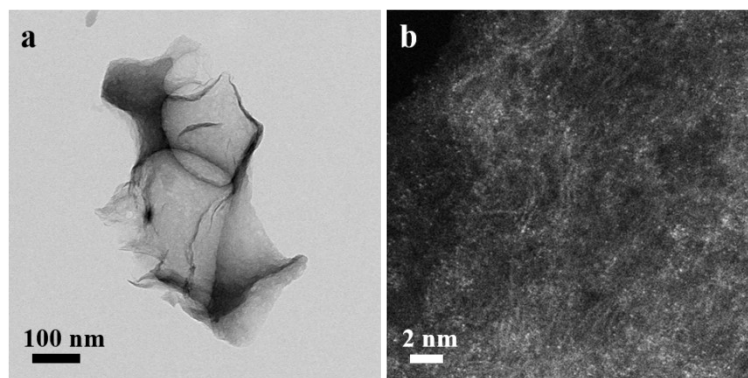


Fig. S20. (a) TEM and (b) AC HAADF-STEM image of SAs-Fe/N-CNSs after durability tests.

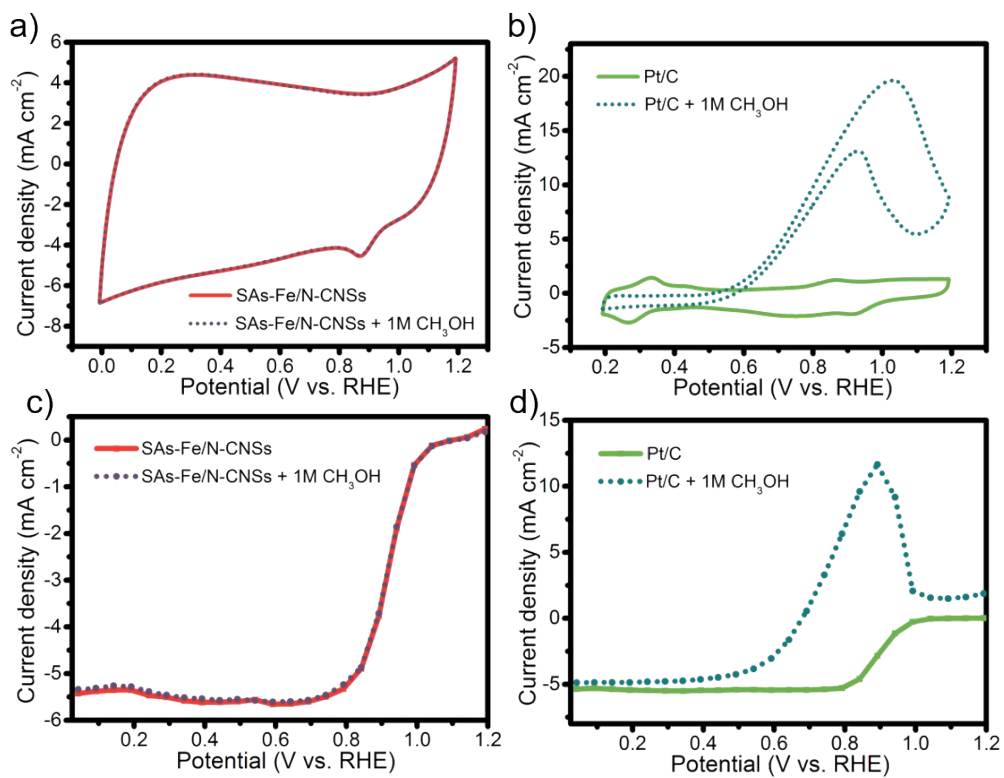


Fig. S21. CV curves of (a) SAs-Fe/N-CNSs and (b) commercial Pt/C in O₂-saturated 0.1 M KOH electrolyte with and without methanol. SCV curves of (c) SAs-Fe/N-CNSs and (d) commercial Pt/C in O₂-saturated 0.1 M KOH electrolyte with and without methanol.

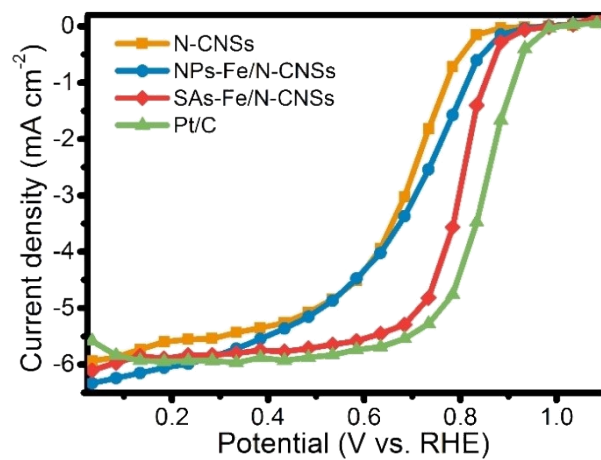


Fig. S22. (a) SCV curve of N-CNSs, NPs-Fe/N-CNSs, SAs-Fe/N-CNSs, and Pt/C on a rotating disk electrode (1600 rpm) in O₂-saturated 0.5 M H₂SO₄.

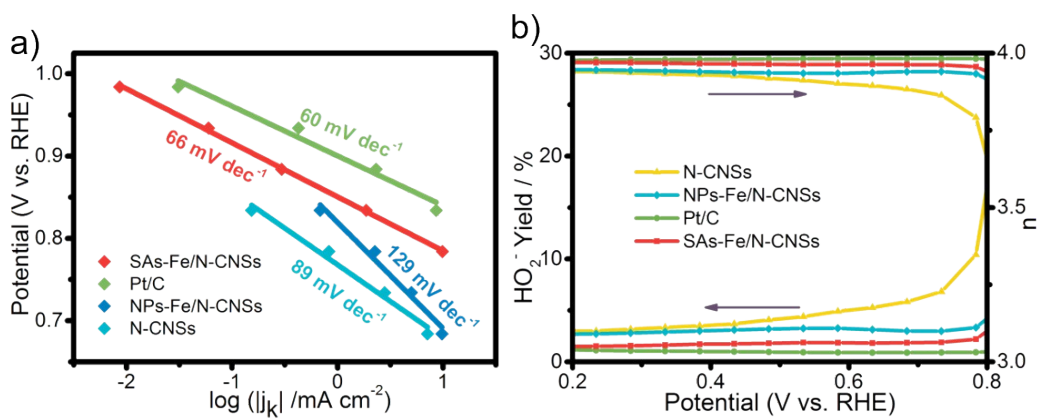


Fig. S23. (a) Tafel slopes and (b) Hydrogen peroxide yield and electron-transfer numbers of SAs-Fe/N-CNSs, Pt/C, NPs-Fe/N-CNSs, and N-CNSs in O_2 -saturated 0.5 M H_2SO_4 solution.

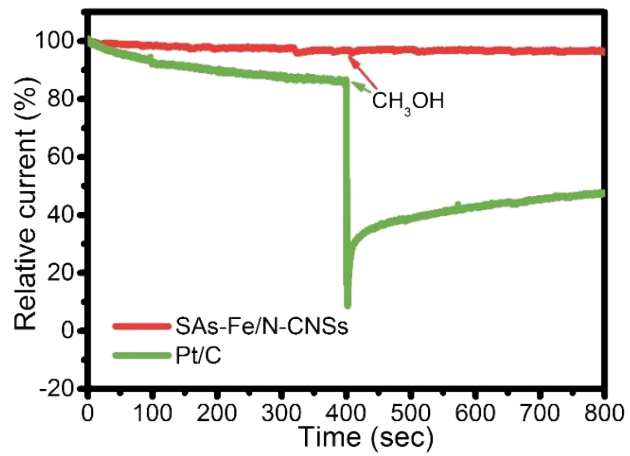


Fig. 24. The *i-t* curves of SAs-Fe/N-CNSs and Pt/C with the addition of CH₃OH at 400 s under acidic condition.

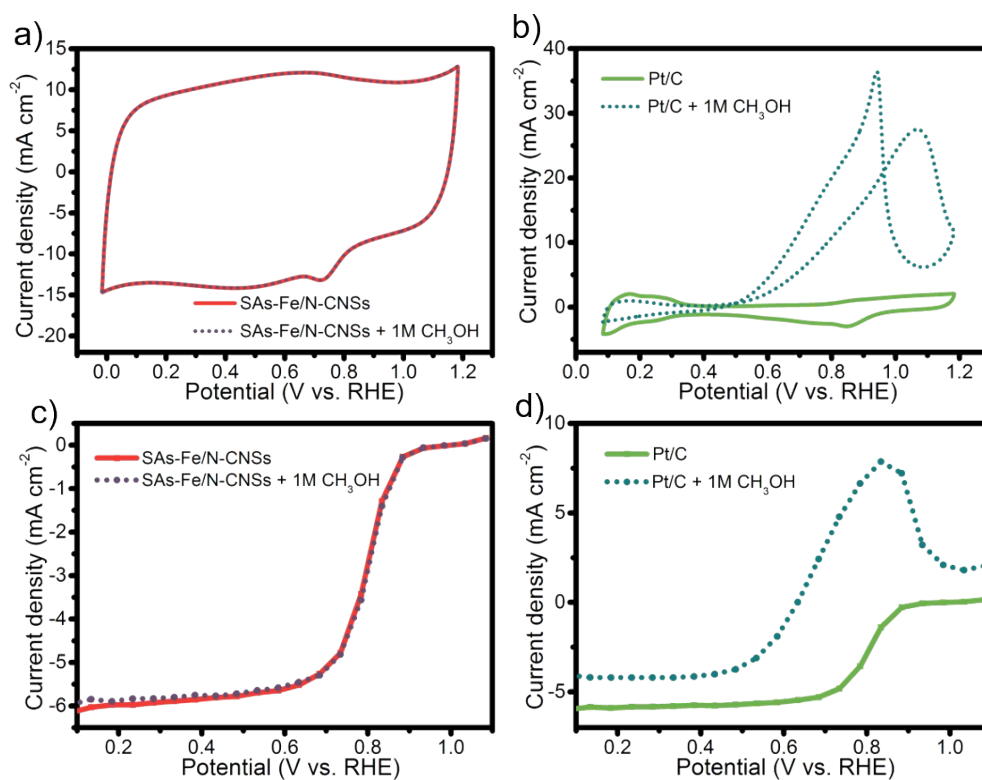


Fig. S25. CV curves of (a) SAs-Fe/N-CNSs and (b) commercial Pt/C in O_2 -saturated $0.5\text{ M H}_2\text{SO}_4$ electrolyte with and without methanol. SCV curves of (c) SAs-Fe/N-CNSs and (d) commercial Pt/C in O_2 -saturated $0.5\text{ M H}_2\text{SO}_4$ electrolyte with and without methanol.

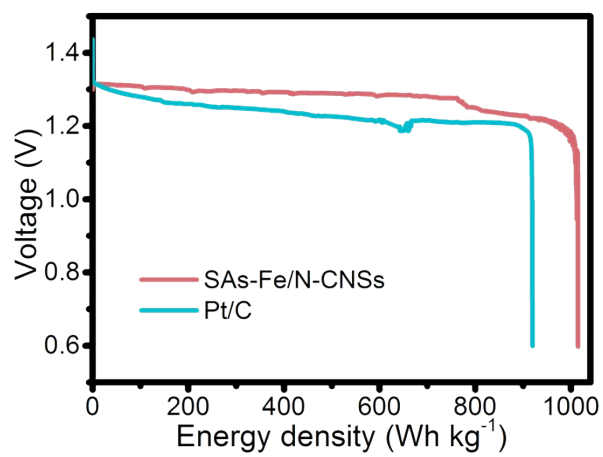


Fig. S26. Specific energy density curves of (a) SAs-Fe/N-CNSs- and (b) commercial Pt/C-based Zn-air batteries.

Table S1. Elemental composition of the catalysts measured by XPS

Sample	C content (at%)	N content (at%)	O content (at%)	Fe content (at%)
SAs-Fe/N-CNSs	84.86	5.78	9.12	0.24
NPs-Fe/N-CNSs	87.91	6.81	4.65	0.63

Table S2. The contents of different elements measured by ICP

Sample	Fe loading (wt%)
SAs-Fe/N-CNSs-0	1.14
SAs-Fe/N-CNSs-1	1.23
SAs-Fe/N-CNSs-2	2.19
SAs-Fe/N-CNSs-4	1.82

Table S3. BET surface area and Total pore volume of the samples measured by N₂ adsorption-desorption experiments.

Sample	BET surface area (m ² g ⁻¹)	Total pore volume (cm ³ g ⁻¹)
SAs-Fe/N-CNSs-0	397.56	0.24
SAs-Fe/N-CNSs-1	435.36	0.26
SAs-Fe/N-CNSs-2	1060.80	0.73
SAs-Fe/N-CNSs-4	537.49	0.37
NPs-Fe/N-CNSs	481.40	0.36
N-CNSs	879.41	0.55

Table S4. Comparison of ORR performance for SAs-Fe/N-CNSs with other reported Fe-based electrocatalysts in alkaline/acid electrolyte.

Catalysts	Electrolyte	Half-wave potential (V vs. RHE)	References
SAs-Fe/N-CNSs	0.1 M KOH	0.91	This work
	0.5 M H ₂ SO ₄	0.801	
Fe _{SA} -N-C	0.1 M KOH	0.90	Nat. Commun. 2020, 11, 2831 ¹
	0.1 M HClO ₄	0.80	
FeSAs/PTF-600	0.1 M KOH	0.87	ACS Energy Lett. 2018, 3, 883-889 ²
FeSA-N-C	0.1 M KOH	0.891	Angew. Chem. Int. Ed. 2018, 57, 8525-8529 ³
	0.1 M HClO ₄	0.776	
2D Fe-NG	0.1 M KOH	0.86	Chem. Eng. J. 2021, 411, 128492 ⁴
Fe SAC-MIL101-1000	0.1 M KOH	0.94	Adv. Mater. 2021, 33, 2101038 ⁵
	0.5 M H ₂ SO ₄	0.80	
3DOM Fe-N-C-900	0.1 M KOH	0.875	Nano Energy 2020, 71, 104547 ⁶
	0.1 M HClO ₄	0.784	
Fe@MNC-1	0.1 M KOH	0.88	ACS Appl. Mater. Interfaces 2019, 11, 25976-25985 ⁷
	0.1 M HClO ₄	0.78	
Fe-N/GNs	0.1 M KOH	0.903	Small Methods

	0.1 M HClO ₄	0.837	2020, 4, 1900827 ⁸
Fe-N-G	0.1 M KOH	0.876	Adv. Mater. Interfaces 2021, 8, 2001788 ⁹
	0.1 M HClO ₄	0.702	

Table S5. Comparison of Zn-air battery performance for SAs-Fe/N-CNSs with other reported Fe-based electrocatalysts.

Catalysts	Peak power density (mW cm ⁻²)	References
SAs-Fe/N-CNSs	157.03	This work
Fe/N-G-SAC	120	Adv. Mater. 2020, 32, 2004900 ¹⁰
Fe-AC-2	153	J. Mater. Chem. A 2021, 9, 7137-7142 ¹¹
Fe-N _x -C	96.4	Adv. Funct. Mater. 2019, 29, 1808872 ¹²
Fe-N-HPC	164.8	J. Mater. Chem. A 2021, 9, 9761-9770 ¹³
A-Fe-NC	132.2	Chem. Eng. J. 2021, 426, 127345 ¹⁴
Fe _x N/NC-7	180	Applied Catalysis B: Environmental 2020, 268, 118405 ¹⁵
mPCN-Fe	153	Nanoscale, 2021, 13, 13249-13255 ¹⁶
FePc@N,P-DC	120	Applied Catalysis B: Environmental 2020, 260, 118198 ¹⁷
A-FeNC	102.2	Phys. Chem. Chem. Phys. 2020, 22, 7218-7223 ¹⁸

References

1. L. Jiao, R. Zhang, G. Wan, W. Yang, X. Wan, H. Zhou, J. Shui, S.-H. Yu and H.-L. Jiang, *Nat. Commun.*, 2020, **11**, 2831-2837.
2. J.-D. Yi, R. Xu, Q. Wu, T. Zhang, K.-T. Zang, J. Luo, Y.-L. Liang, Y.-B. Huang and R. Cao, *ACS Energy Lett.*, 2018, **3**, 883-889.
3. L. Jiao, G. Wan, R. Zhang, H. Zhou, S. H. Yu and H. L. Jiang, *Angew. Chem. Int. Ed. Engl.*, 2018, **57**, 8525-8529.
4. C. Wang, Y. Liu, Z. Li, L. Wang, X. Niu and P. Sun, *Chem. Eng. J.*, 2021, **411**, 128492.
5. X. Xie, L. Peng, H. Yang, G. I. N. Waterhouse, L. Shang and T. Zhang, *Adv. Mater.*, 2021, **33**, 2101038.
6. X. Zhang, X. Han, Z. Jiang, J. Xu, L. Chen, Y. Xue, A. Nie, Z. Xie, Q. Kuang and L. Zheng, *Nano Energy*, 2020, **71**, 104547.
7. X. Chen, N. Wang, K. Shen, Y. Xie, Y. Tan and Y. Li, *ACS Appl. Mater. Interfaces*, 2019, **11**, 25976-25985.
8. D. Liu, J.-C. Li, S. Ding, Z. Lyu, S. Feng, H. Tian, C. Huyan, M. Xu, T. Li, D. Du, P. Liu, M. Shao and Y. Lin, *Small Methods*, 2020, **4**, 1900827.
9. S. Zhao, L. Zhang, B. Johannessen, M. Saunders, C. Liu, S.-Z. Yang and S. P. Jiang, *Adv. Mater. Interfaces*, 2021, **8**, 2001788.
10. M. Xiao, Z. Xing, Z. Jin, C. Liu, J. Ge, J. Zhu, Y. Wang, X. Zhao and Z. Chen, *Adv. Mater.*, 2020, **32**, 2004900.
11. Y. Wang, Q. Li, L.-c. Zhang, Y. Wu, H. Chen, T. Li, M. Xu and S.-J. Bao, *J. Mater. Chem. A*, 2021, **9**, 7137-7142.
12. J. Han, X. Meng, L. Lu, J. Bian, Z. Li and C. Sun, *Adv. Funct. Mater.*, 2019, **29**, 1808872.
13. D. Wang, H. Xu, P. Yang, L. Xiao, L. Du, X. Lu, R. Li, J. Zhang and M. An, *J. Mater. Chem. A*, 2021, **9**, 9761-9770.
14. N. Shang, C. Wang, X. Zhang, S. Gao, S. Zhang, T. Meng, J. Wang, H. Wang, C. Du, T. Shen, J. Huang, Y. Qiao, Q. Wu and Y. Gao, *Chem. Eng. J.*, 2021, **426**, 127345.
15. X. Hu, Y. Min, L.-L. Ma, J.-Y. Lu, H.-C. Li, W.-J. Liu, J.-J. Chen and H.-Q. Yu, *Appl. Catal. B*, 2020, **268**, 118405.
16. J. Ding, D. Wu, S. Huang, C. Lu, Y. Chen, J. Zhang, L. Zhang, J. Li, C. Ke, D. Tranca, E. Kymakis and X. Zhuang, *Nanoscale*, 2021, **13**, 13249-13255.
17. W. Cheng, P. Yuan, Z. Lv, Y. Guo, Y. Qiao, X. Xue, X. Liu, W. Bai, K. Wang, Q. Xu and J. Zhang, *Appl. Catal. B*, 2020, **260**, 118198.
18. M. Lv, H. Guo, H. Shen, J. Wang, J. Wang, Y. Shimakawa and M. Yang, *Phys. Chem. Chem. Phys.*, 2020, **22**, 7218-7223.